Physics – Uspekhi **60** (3) 305 – 318 (2017)

METHODOLOGICAL NOTES PACS numbers: 07.05.Tp, **61.72. – y**, **62.20. – x**

Dislocation kinetics in nonmagnetic crystals: a look through a magnetic window

V I Alshits, E V Darinskaya, M V Koldaeva,
R K Kotowski, E A Petrzhik, P Tronczyk

DOI: https://doi.org/10.3367/UFNe.2016.07.037869

Contents

Abstract. We discuss new kinematic magnetoplasticity features established experimentally and by simulations. We examine the motion of a dislocation through randomly distributed point defects under the influence of a magnetic field that reduces the impurity pinning forces. In addition to the measurable characteristics of motion, hidden motion parameters amenable only to simulation studies are investigated for the first time. It is shown that the distribution of stoppers on a dislocation is independent of the impurity concentration C, whereas the average number of stoppers and the critical force for the dislocation breakaway are proportional to $\sqrt{C}$. A model is proposed that for the first time explains the observed concentration dependence of the average dislocation speed in a magnetic field, $v \propto 1/\sqrt{C}$. The model suggests that there is hidden room for an orders-of-magnitude increase in v, something which was already realized in NaCl crystals additionally subjected to a weak electric field.

Keywords: magnetoplastic effect, dislocation, impurity defect, pinning center, magnetic field, electric field, computer simulation

V I Alshits, E V Darinskaya, M V Koldaeva, E A Petrzhik
Shubnikov Institute of Crystallography of Federal Scientific Research Center 'Crystallography and Photonics', Russian Academy of Sciences, Leninskii prosp. 59, 119333 Moscow, Russian Federation
Tel. (7-495) 330 82 74. Fax (7-499) 135 10 11
E-mail: alshits@ns.crys.ras.ru
R K Kotowski, P Tronczyk Polish–Japanese Academy of Information Technology, ul. Koszykowa 86, 02-008 Warsaw, Poland
Tel. (48-22) 58 44 560. Fax (48-22) 58 44 501
E-mail: rkotow@pja.edu.pl

Received 20 June 2016
Uspekhi Fizicheskikh Nauk **187** (3) 327 – 341 (2017)
DOI: https://doi.org/10.3367/UFNr.2016.07.037869
Translated by S N Gorin; edited by A M Semikhatov

1. Introduction

The magnetoplastic effect (MPE) was discovered in [1] as the motion of dislocations in NaCl crystals held in a DC magnetic field $B \approx 0.5$ T in the absence of a mechanical load. It became clear already in early studies [1–3] that the driving force for the motion of dislocations under these conditions is the presence of internal stresses that act on so-called fresh dislocations that are introduced directly before the beginning of the experiment and become retarded in nonequilibrium positions on impurity stoppers. The role of the magnetic field reduces to changing the structure of these stoppers, which ensures a decrease in the force of pinning the dislocations. It was supposed in [3, 4] that this transformation can occur as a result of the evolution of spin configurations at the centers on dislocations into a state that eliminates the quantum exclusion of some specific electron transitions in the system, which in turn produces a rearrangement of the center and a change

in the dislocation pinning force. Similar spin-dependent processes are well known in chemical physics [5, 6].

Active studies of the MPE by a number of independent research groups have led to significant clarity in the understanding of the physical nature of this phenomenon (see reviews [7–11]). The spin-related hypothesis was confirmed experimentally [12–14]. A similar effect was revealed in other alkali-halide crystals (AHCs) [15], nonmagnetic metals Zn [16] and A1 [17], semiconductor InSb [18], and later in many other materials. Macroscopic manifestations of the MPE were revealed in the case of an active loading ($\dot{\sigma} = \text{const}$) [19], active straining ($\dot{\varepsilon} = \text{const}$) [20], creep ($\sigma = \text{const}$) [21], and internal friction [22] in crystals.

In some crystals, an effect of magnetic memory was revealed [23, 24] in addition to the usual MPE. In such crystals, the magnetic field modifies the impurity centers in the bulk of a material, which for some time changes the mechanical properties of the sample. In the experiments performed, there were fixed changes in the mobility of dislocations [24] introduced into an NaCl crystal already after its magnetic exposure, and also in the microhardness of many crystals, e.g., AHCs [23, 25], semiconductors (ZnS [26], InSb and CdTe [27], ZnO [28]), and molecular crystals (fullerene [29] and potassium hydro-phthalate [30]).

An achievement of fundamental importance was the discovery of the resonance MPE, when the magnetic treatment of a crystal is realized in the scheme of electron paramagnetic resonance (EPR) under the joint action of two crossed magnetic fields, DC and AC. The resonance occurs if the frequency ν of the AC field corresponds to the Zeeman splitting $\Delta E = h\nu$ of the spin levels in the DC magnetic field. At the standard EPR frequency $\nu \approx 10$ GHz, such resonances were observed in AHCs [13, 14] and silicon [31, 32] in the *in situ* regime [13, 14] and in the regime of the memory effect [14, 31, 32] from changes in the motion of both individual dislocations [13, 14, 31, 32] and macroplasticity and microhardness of crystals [14]. These results were a direct confirmation of the spin-dependent nature of magnetoplasticity.

Recently, the resonance MPE was detected in the range of radio frequencies $10^4 - 10^6$ Hz when using the terrestrial magnetic field ($\approx 10^{-4}$ T) at individual dislocations in NaCl [33–35] and based on changes in the microhardness of crystals of zinc oxide (ZnO), triglycine sulfate, and potassium hydrophthalate [36]. The degree of the modification of the plastic properties of crystals as a result of their exposure in ultralow magnetic fields proved to be much the same as when holding the same crystals in a DC field $B \approx 1$ T.

A similar dislocation-related resonance in the terrestrial magnetic field was also revealed in NaCl crystals upon *pulsed* pumping [37]. A narrow peak of path lengths with a maximum at the pulse duration $\tau_r \approx 0.53$ μs was observed, which corresponds to the normal condition of EPR, when the frequency is equal to $1/\tau_r$. The motion of dislocations under such conditions is in fact an *ultrafast coherent relaxation*. In this case, the dislocations travel distances of ~ 100 μm in a time of 0.5 μs as during the harmonic pumping with an exposure for 5 min.

It turns out that the low-frequency resonance differs significantly from its high-frequency analog. The low-frequency resonance is strongly anisotropic, and its frequency depends on the orientation of the sample relative to Earth's magnetic field. Based on these phenomena, a new method of EPR spectroscopy of dislocation paths $l(\nu)$ is being developed [38–41]. In particular, for NaCl crystals, a large series of $l(\nu)$ peaks was found in the frequency range 10–550 kHz [39, 40], each connected with a specific position of the impurity center in the dislocation core. Thus, varying the pumping frequency, it is possible to selectively transform the pinning centers in any structural positions.

To date, a significant amount of experimental data concerning magnetoplasticity has been accumulated, which allows interpreting many of its manifestations not only on the level of qualitative reasoning. Theoretical models already exist that describe many experimental dependences on different physical parameters [11]. Even very fine spin processes are gradually becoming clear [11, 33, 39, 42–51]. This also concerns the less studied effects of magnetic memory, which in recent years have also been actively discussed and analyzed [36, 52–54].

The difficulties in describing the kinetics of magnetoplasticity are connected with the limitations of the methods for observing such processes as a result of the different scales of the macroeffects studied and related spin-dependent transformations of the structure of impurity centers that cause these effects. In fact, even measurements of the displacements of an individual dislocation in a magnetic field give only indirect information about the kinetics of the process. Such measurements are based on selective etching of the crystal surface. In experiment, the path of a dislocation is fixed as the distance between the etching pits that mark the initial and final positions. All components of the dislocation movement, such as the kinetics of depinning from point defects, and statistics of dislocation segments, remain unknown and can be restored only from indirect data. Fortunately, these data are quite various and, as we see in what follows, some fine details of the kinetics of dislocation motion can nevertheless be understood and explained.

Certainly, it is impossible to completely overcome the limitations of a method of experimental observations. But it can be supplemented with theoretical modeling and computer simulations of the motion of dislocations through a random network of obstacles. The old idea of the method of simulations, in spite of its own limitations even with the capabilities of modern-day computers, has an important merit: from computer experiments, it is indeed possible to extract many details inaccessible in real physical experiments [55]. Below, we describe numerical experiments and build a bridge between the data obtained by measurements and by computer simulation. Conclusions obtained in this article are equally applicable to both methods of the magnetic action on the crystal: by using a DC magnetic field and by the application of an EPR resonance scheme.

2. Physics of solid-state reactions in a magnetic field

The magnetoplastic effect belongs to a relatively new group of phenomena caused by the influence of weak magnetic fields on the rate of the processes of interaction of paramagnetic particles (radicals, electrons, etc.) and on chemical reactions in which they participate. All such effects are limited by the principle of spin selectivity: the reactions are allowed only from definite spin states. The spin interactions with the magnetic fields, although negligible in energy, have a strong effect on the physical result of the process, changing the spin state of the system and thus eliminating spin exclusions. For this reason, low-energy magnetic interactions can greatly influence chemical reactions, luminescence, electrical con-

ductivity, photosynthesis, etc. We speak here of various phenomena that were being studied independently in different research fields: in the physics of molecular crystals, chemical kinetics, physics of semiconductors, etc. (for more details, see, e.g., Ref. [6]).

The magnetoplasticity, i.e., the initiation of dislocation motion by a magnetic field, can be regarded as a 'magnetic catalysis' of dislocations [46]. Numerous diverse experiments have proved that the key unit, the source of this catalysis, is the dislocation + stopper system. Because it makes no sense to speak of a significant contribution of a magnetic field to the energy characteristics of this system, we should recognize that the electron spin plays a key role here one way or another, and a spin-selective nanoscale reactor arises, in which spin exclusions controlled by a magnetic field exists.

When speaking of a stopper, we mean an impurity complex in the dislocation core, which contains a radical-type pair of electrons, which in a magnetic field changes the spin state such that the quantum exclusion of a particular electron transition in the system is eliminated. This, in turn, leads to a reconstruction of the complex that corresponds to a reduction in the pinning force and a depinning of the dislocation under the action of internal stresses existing in the crystal. The new structure of the complex usually proves to be long-lived. In an NaCl crystal, according to [56], the transformed pinning center after the breakaway of the dislocation returns to the initial structural state only in 7–10 min. In Section 3.3, we consider possible scenarios of the spin-dependent transformation of stoppers in such crystals in more detail.

As with other phenomena [6] based on spin-selective reactions in a magnetic field, processes of this type occur only under specific conditions. In particular, the time of the spin evolution (in our case, the depinning time τ_{dp}) in the system must always be small in comparison with the spin–lattice relaxation time τ_{s-l}. Otherwise, the thermal chaotization of spins makes the reactions that are of interest for us practically impossible. Because the time τ_{dp}, according to our data, increases with a reduction in the magnetic field, there must be a threshold field B_{th} at which the magnetoplasticity is suppressed in smaller fields as well. The magnitude of the threshold field is estimated from the condition $\tau_{dp}(B_{th}) \sim \tau_{s-l}$. As is known, the time τ_{s-l} increases as the temperature decreases; this should lead to a decrease in B_{th}. In Ref. [12], such threshold fields for the existence of magnetoplasticity were revealed and measured for a number of crystals. Their expected behavior with a change in the temperature was also confirmed.

3. Properties of the magnetoplastic effect

3.1 Measurement procedure

The dislocations in AHCs 'age' rapidly: they diffusionally become surrounded by point defects (by so-called Cottrell atmospheres) and become low-mobile. Therefore, the experiments described are conducted only using fresh dislocations, which are introduced into the crystal by a light impact. The dislocations in this case are rectilinear ($\parallel [100]$), and their density ρ_{fr} is usually comparable with the density ρ_{old} of the old dislocations: $\rho_{fr} \approx \rho_{old} \approx 10^4$ cm^{-2}. After the impact, the dislocations run away from the sources and stop in those places where internal stresses cannot overcome the pinning force of impurity centers.

Before the introduction of new dislocations, the surfaces of the crystal are subjected to chemical etching in order to determine the positions of old dislocations. After the impact, repeated etching is performed to determine the starting positions of fresh dislocations. Then the crystal is placed into a magnetic field, and after exposure it is etched again in order to determine the final positions of the displaced dislocations. Then the histograms of dislocation paths are constructed and the mean paths l of the dislocations are calculated. Furthermore, the average density ρ_m of mobile dislocations is measured. The dependences of these two quantities on various physical parameters (exposure time, magnetic induction, concentration of impurities, temperature, etc.) are the aim and the result of such experiments.

3.2 Dependence of the magnetoplastic effect on the basic physical parameters

According to measurement data, the mean path l and the density ρ_m of mobile dislocations increase monotonically with an increase in the product B^2t and are usually described well by the empirical dependences [1–3, 7, 11]

$$\begin{aligned} &\Delta l \equiv l - l_0 \approx kB^2t\,, \\ &\Delta\rho_m \equiv \rho_m - \rho_0 \approx \Delta\rho_\infty\left[1 - \exp\left(-\lambda B^2t\right)\right], \end{aligned} \tag{1}$$

where l_0 and ρ_0 are the background values of the parameters connected with the etching away of near-surface stoppers; $\Delta\rho_\infty = \rho_m - \rho_0$ as $B^2t \to \infty$; and k and λ are constants characteristic of a given crystal.

Figure 1 shows the dependences of dislocation paths and densities of mobile dislocations on B^2t measured using a series of NaCl crystals with different concentrations C of an impurity of Ca. As can be seen from the figure, the results of the calculation via formulas (1) agree quite well with the experimental data. In this case, the parameters k and λ are proportional to $1/\sqrt{C}$ (see the insets in Fig. 1). We note that the linear dependence of the mean path l on B^2t presented in Fig. 1a saturates upon further growth of the magnetic field B and time t (not shown in the figure), retaining a practically constant value of the mean path $l \sim 1/\sqrt{\rho}$ at the level of the order of the mean distance between dislocations, just as it should be in the case of relaxation of internal stresses in the crystal determined by the entire totality of dislocations with the density $\rho = \rho_{fr} + \rho_{old}$.

Both these quantities, l and ρ_m, are only weakly sensitive to the effect of temperature. As the temperature decreases from room values to 77 K, the mean path l decreased by only 20%, and the further decrease in the temperature to 4 K had no significant effect on the path [2, 7, 11]. This indicates that the thermoactivation processes do not play a decisive role in the MPE mechanisms.

3.3 Paradox of the influence of the impurity of calcium

Most information about the kinematics of magnetoplasticity was obtained in experiments on the crystals of NaCl. As a result, NaCl became a convenient model object for the study of MPE. The basic strengthening impurity in NaCl crystals is usually calcium. Being bivalent, the atoms of Ca enter the NaCl crystal in the form of Ca^{2+} ions, which substitute for Na^+ ions. For the local electroneutrality of the lattice to be retained, the calcium ions and negatively charged sodium vacancies form dipoles:

$$Ca^{2+} + V^-_{Na} = Ca^{2+}V^-_{Na}\,. \tag{2}$$

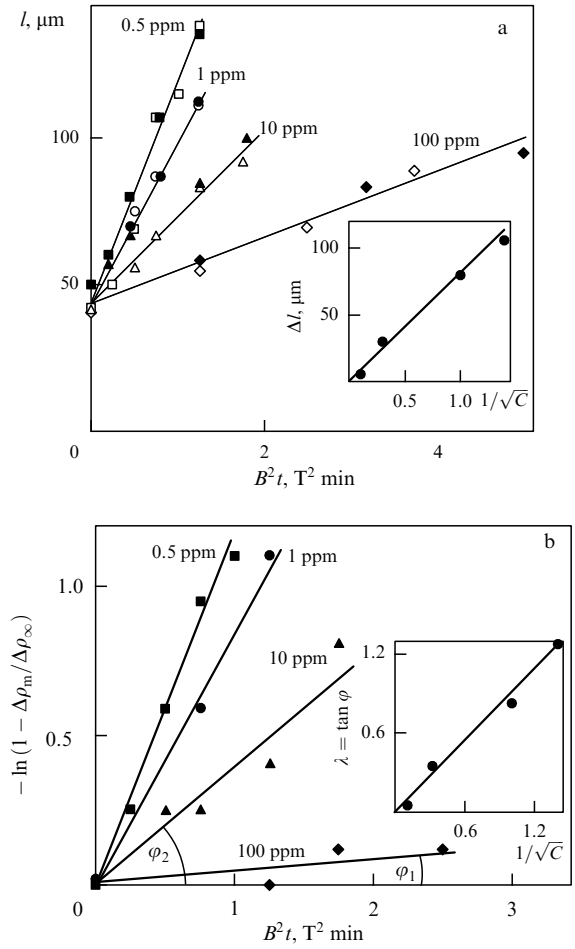

Figure 1. Dependence of (a) the mean path l and (b) the relative density $\Delta\rho_m/\Delta\rho_\infty$ of mobile dislocations in NaCl(Ca) crystals on the magnetic induction B and the time t of holding the samples in the magnetic field (B^2t). In the insets in Figs 1a and 1b, the dependences are given of the increase in the path Δl and the slopes $\lambda = \tan\varphi$ of the straight lines (shown in Fig. 1b) on the concentration C of Ca impurities at $B = 0.5$ T.

The dissociation energy of these dipoles in the bulk of the crystal is ~ 0.27 eV [57]. It is known that these dipoles travel through the crystal by diffusion as a whole unit.

The fact that it is precisely calcium that determines the MPE in the NaCl(Ca) crystal is beyond question. The measured mean path l of dislocations in such crystals placed in a magnetic field definitely depends on the Ca concentration C [3, 7, 11] (Fig. 1a):

$$\Delta l \propto \frac{1}{\sqrt{C}}\,. \tag{3}$$

However, the $Ca^{2+}V_{Na}^-$ dipole is diamagnetic and cannot participate in spin-dependent reactions. This paradox led to a discussion in the literature [58] and finally resulted in the following physical interpretation. The idea is that only those Ca atoms that fall into the dislocation core become magnetically active, i.e., the transformation $Ca^{2+} \to Ca^+$ occurs there. The question remains: how and why does this occur?

A model by Buchachenko appeared first [46], based on an elegant idea of the generation of a two-spin magnetically sensitive nanoreactor in a dislocation trapped by a stopper due to the transfer of an electron from a Cl_d^- ion in the dislocation core onto the impurity ion of Ca^{2+}. As a result,

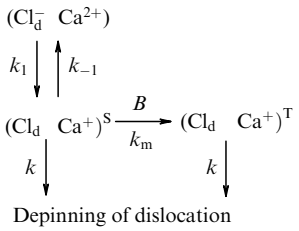

Figure 2. Diagram of the motion of dislocations.

two unpaired electrons appear, one on the dislocation and the other on the stopper, and thus a spin nanoreactor arises with singlet and triplet spin states. As in the case of any thermally or mechanically induced process, the transfer of the electron occurs without a change in spin, and the new pair $(Cl_d\ Ca^+)^S$ is in the singlet state S, from which the reverse transfer of the electron is allowed (Fig. 2).

Moreover, such a process is even preferable (i.e., $k_{-1} \gg k_1$ in the diagram presented in Fig. 2). However, the magnetic field B initiates the spin conversion of the pair $(Cl_d\ Ca^+)^S$ from the singlet state into the triplet state $(Cl_d\ Ca^+)^T$, in which the reverse transfer of the electron is spin-forbidden. We note an important circumstance: in the new $(Cl_d\ Ca^+)$ pair, Coulomb interaction is absent. This is possibly why the pinning force decreases sharply and dislocation is depinned and continues moving.

An advantage of this model is a convincing demonstration of the principle of spin-selective reaction in the dislocation–stopper system. As regards its correspondence to the observed magnetoplasticity properties, which we discuss below, some problems remain. For example, this model does not explain the enormous increase (by three orders of magnitude!) in the velocity of dislocations in a magnetic field under the additional action of a relatively weak electric field on the crystal (see Section 4.3). Apparently, when constructing the model, we should not ignore the above-noted fact that we are dealing with a $Ca^{2+}V_{Na}^-$ dipole rather than with a Ca^{2+} ion. As we see below, the presence of the vacancy V_{Na}^- in this dipole plays the key role in the electrostimulation of magnetoplasticity.

To explain the observed properties, the following alternative model was proposed in [11, 49, 50]. Near the dislocation core, the vacancy V_{Na}^- is pulled onto the edge of the dislocation extra half plane; more precisely, under the action of enormous pressure, the Na^+ ion is pushed out from there into a vacant position near Ca^{2+}. In this case, for electroneutrality to be retained, the Cl^- anion (located at the same edge of the extra half plane) that is nearest to the captured vacancy V_{Na}^- gives an electron back to the Ca^{2+} ion with the formation of a magnetically active cation Ca^+ (as in the model suggested in [46]). The reverse transition is excluded simply because of the Coulomb repulsion. There are experimental grounds to assume that after this the neutral Cl^0 atom and the neighboring Cl^- anion form a covalent V-center — a charged molecule Cl_2^- — in the dislocation core. As a result, a magnetically active complex $Ca^+\,Cl_2^-$ appears in the dislocation, which contains a radical pair of spins, whose magnetic transformation is completed by the reaction

$$Ca^+ + Cl_2^- = CaCl_2\,. \tag{4}$$

The new pinning center — the covalent molecule $CaCl_2$ — is electrically neutral, and this may be the reason why it interacts

more weakly with the dislocation core in the ionic crystal. On the other hand, this molecule is magnetically nonactive and is very stable, which correlates with the above-mentioned data [56], according to which upon repeated application of a magnetic pulse to the NaCl crystal, the MPE is restored in only 7 to 10 min.

An indirect confirmation of the validity of the mechanism under discussion is also the recently discovered significant increase in the density of free cation vacancies in LiF crystals after their exposure in a magnetic field [59].

3.4 Relay-race mechanism of dislocation motion

The growth in the density of mobile dislocations with an increase in the time of the exposure of the sample in a magnetic field (Fig. 1b) indicates a relay-race mechanism of their motion. Indeed, the movement of dislocations in the described experiments is a kind of relaxation self-organization accompanied by a decrease in the elastic energy in the crystal. The dislocations move downward along the slopes of the potential relief of the internal stresses created by the entire dislocation ensemble, from the more stressed regions to those less stressed. This reduces the total elastic energy but increases the level of local stresses in those places into which the dislocations come. As a result, the incoming dislocations stimulate the motion of other dislocations that have either not yet moved or already stopped because of the insufficiently high level of stresses. This is the essence of the relay-race type of motion of dislocations. In experiments, apparently, this is often the mechanism that gradually involves almost all fresh dislocations into motion.

It is obvious that in the case of such relay-race-type displacements, the average time t_m of motion of a separate dislocation should be considerably less than the time t of the exposure of the crystal in the magnetic field. In Ref. [3], in the framework of a simple model, besides formulas (1), it was also found that the time t_m is approximately $t/6$. In reality, judging from indirect data, t_m is even a fraction of that. For example, in [11] it is assumed that

$$t_m \approx \frac{t}{15} . \tag{5}$$

4. Physical model of the kinematics of the process

4.1 Paradox of the slowness of motion

We now discuss the possible physical meaning of empirical dependences (1) and (3) in the concept of a mean path l of a dislocation. The linearity of the dependence of l on the time t (with not too large values of $B^2 t$) indicates that we are dealing with stationary motion, which can be described by a constant mean velocity

$$v \propto \frac{B^2}{\sqrt{C}} . \tag{6}$$

In [1–3], in NaCl(Ca) crystals with the calcium concentration $C = 0.5$ parts per million (ppm) and the time $t = 5$ min of the sample exposure in the magnetic field $B = 0.5$ T, the mean free path of dislocations was $\Delta l \sim 100$ μm (Fig. 1a), i.e., the average velocity of dislocations was ~ 0.3 μm s^{-1}. However, taking Eqn (5) into account, the true mean velocity is much higher:

$$v \sim 5 \text{ μm s}^{-1} . \tag{7}$$

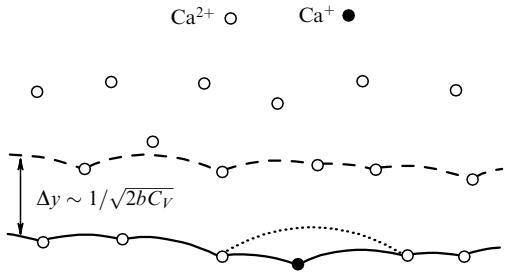

Figure 3. Starting position of a dislocation (solid curve) and its position when pinned by the next row of stoppers (dashed curve). The dotted segment shows the first breakaway of the dislocation from a magnetically active center (black dot) after the application of a magnetic field and the beginning of the propagation of two unzipping cascades (to the left and to the right).

For a physical interpretation of relation (6) and of estimate (7), we pass from the simple and convenient and, above all, observable object — an etching pit on a crystal surface — to a much more complex image of a dislocation that moves through a random network of point defects (impurity centers). Figure 3 schematically shows two positions of a dislocation, which correspond to its passage from one 'row' of stoppers to another. These positions are separated by a distance $\Delta y \sim 1/\sqrt{2bC_V}$. Here, b is the length of the Burgers vector, which is of the order of the lattice parameter; $2b$ is the 'thickness' of the slip plane; and C_V is the volume concentration of impurity centers, which differs from C only by a dimensional coefficient. Let Δt be the time necessary for the above-mentioned passage of the dislocation. Its velocity is then given by

$$v \sim \frac{\Delta y}{\Delta t} . \tag{8}$$

It can be easily shown (see [7, 11]) that in an NaCl(Ca) crystal with the calcium concentration $C = 0.5$ ppm ($C_V \sim 10^{17}$ cm^{-3}) and a distance Δy between the rows of stoppers (see Fig. 3), the following estimate is valid:

$$\Delta y \sim \frac{1}{\sqrt{2bC_V}} \sim 0.3 \text{ μm} . \tag{9}$$

Taking Eqns (7) and (8) into account, the following time is required for such a displacement of the dislocation:

$$\Delta t \sim 0.06 \text{ s} . \tag{10}$$

This time is too large for assigning it to the spin evolution in the impurity center, which, undoubtedly, limits the time τ_{dp} of the magnetic depinning of the dislocation from a stopper. As has already been said, a necessary condition for spin-dependent transitions is the smallness of this time in comparison with the spin–lattice relaxation time τ_{s-l} in the system ($\tau_{dp} \ll \tau_{s-l}$) [6]; otherwise, the thermal oscillations would randomize the spin system long before the occurrence of the transition. The experimental estimate $\tau_{s-l} \sim 10^{-4} - 10^{-3}$ s [7, 11, 12] for the same crystals, which was obtained taking this condition into account and was recently confirmed in [39], shows that τ_{dp} cannot be more than 10^{-4} s. Thus, the spin-related transformation of defects at the dislocations cannot occur everywhere

simultaneously; this means that it occurs consecutively in many places.

4.2 Idea of unzipping and the completion of the velocity estimate

We assume the validity of the estimate $\tau_{dp} \sim 3 \times 10^{-5}$ s given in Ref. [11] based on the extrapolation of data of measurements performed in [56]. Then the cascade of sequential acts of depinning of dislocations from the pinning centers ('unzipping'), which gives rise to the total time (10), must consist of $n_{unz} \sim \Delta t/\tau_{dp} \sim 10^3$ acts. We show below that in a crystal with the bulk concentration of impurities 10^{17} cm^{-3}, the mean length of a dislocation segment $\bar{x}$ is of the order of 1 μm [see Eqn (26) in Section 5.3]. Therefore, with the total length of a dislocation $L \sim 3$ mm, on average, $n_{tot} \sim 3 \times 10^3$ pinning centers must be located there. This corresponds to only a few unzipping cascades on such a dislocation: $n_{tot}/n_{unz} \approx 3$. The cascades are initiated by the depinning of a dislocation from active centers. Each such center must already be, first, in a magnetically sensitive state (Ca^+) and, second, located in a sufficiently 'weak' part of the dislocation (for example, on a long segment), where the dislocation can be depinned because of a decrease in the pinning force as a result of a magnetic transformation of the center. Further, an 'avalanche-type' release of the dislocation begins. First, because of a sharp lengthening of the segment as a result of the first breakaway, the dislocation is pressed into two adjacent centers and activates calcium ions in them: $Ca^{2+} \rightarrow Ca^+$. Then, after the magnetic transformation of these centers, a breakaway also occurs of the dislocation from these centers, and so on. Each active center launches two unzipping cascades simultaneously, which propagate in opposite directions (in Fig. 3, one active center and the two associated cascades are shown). The lengths of their paths depend on many factors.

In principle, there is nothing exotic in the model under consideration. The phenomenon of unzipping is well known in the theory of thermoactivational dynamics of dislocations. From the estimates obtained, it follows that in our case the mean 'length' of unzipping is very large: $n_{unz} \sim 10^3$, and the mean number of active centers at a dislocation is very small: $n_{act} \approx n_{tot}/2n_{unz} \sim 1$. But these estimates should not be taken literally. The processes discussed vary greatly. For instance, a cascade can be stopped at a defect on which the decrease in the pinning force is insufficient for the depinning (for example, because the segments are too short or there is low internal stress at this place). The dislocation can then experience either the unzipping from the other side of the defect or a relay-race-type approach of another dislocation with an increase in the local level of internal stresses. Finally, the dislocation can no longer move, which reduces the contribution to the mean path l in the histogram of paths. This, in turn, decreases the average velocity of the dislocation and thus increases the mean time (10), which in our model is equivalent to an increase in n_{unz}.

We emphasize that the estimates obtained for the high value of the parameter n_{unz} are based on the experimental data on the velocities of dislocations. They indicate a small number n_{act} of active Ca^+ centers at the dislocation. There is quite a serious reason for this conclusion. Because of the elastic repulsion of a dislocation from an impurity center, they can come sufficiently close to each other, as is necessary for the above-described spontaneous transformation $Ca^{2+} \rightarrow Ca^+$, only in a small number of long segments.

Substituting expressions $\Delta y \sim 1/\sqrt{2bC_V}$ and $\Delta t \sim n_{unz}\tau_{dp} = (n_{tot}/2n_{act})\tau_{dp}$ in Eqn (8), we obtain

$$v \approx \frac{2n_{act}}{n_{tot}\tau_{dp}\sqrt{2bC_V}} = \frac{2w}{\tau_{dp}\sqrt{2bC_V}}\,, \tag{11}$$

where we introduce the probability $w = n_{act}/n_{tot}$ that a given stopper at the dislocation is a center of unzipping. The last quantity, naturally, is independent of the magnetic field B. Therefore, from a comparison of (6) with (11), it can be deduced that $\tau_{dp} \propto B^{-2}$ in our model. In other words, when discussing the physical mechanisms of spin evolution, we should give preference to mechanisms that give the time of spin transition proportional to B^{-2} (see [7, 11, 43]).

4.3 Anomalous electrical stimulation of the magnetoplastic effect as a confirmation of the model

Equation (11) shows that there is significant room for the increase in the velocity v due to an increase in the number n_{act} of active Ca^+ centers in the dislocation core and, accordingly, a shortening of the unzipping cascades. As was shown in [49, 50], the mean velocity v of dislocations in NaCl crystals can indeed be increased substantially with the aid of an electric field E acting simultaneously with a magnetic field (Fig. 4a). First, in the range of electric fields $0 < E < 5$ kV m^{-1}, the velocity is directly proportional to the field ($v \propto E$), increasing approximately sixfold over its value v_0 in a zero field, $E = 0$ (Fig. 4b). Then the linear growth becomes exponential (Fig. 4c): at $E \sim 15$ kV m^{-1}, the velocity v increases by three orders of magnitude compared with v_0. This process clearly has a thermoactivational nature; the activation energy $U_0 \approx 0.2$ eV measured at $E \rightarrow 0$ in the vicinity of the

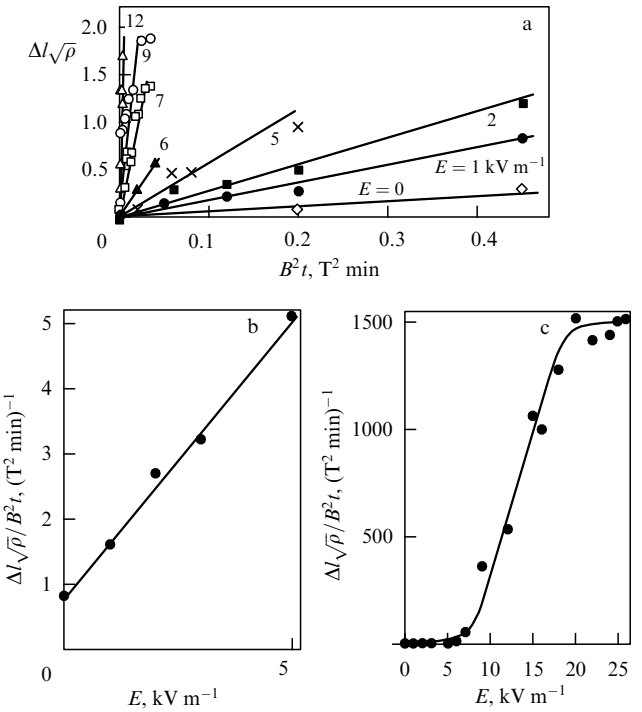

Figure 4. Dependences of the normalized mean path of dislocations Δl in the time of exposure t of NaCl(Ca: 10 ppm) in a magnetic field B and in an electric field E (a) on the product B^2t for several values of E indicated in the figure, and also on the field E at (b) low values of $E < 5$ kV m^{-1} and (c) higher E in a wider interval $E < 25$ kV m^{-1}.

dislocation core is in reasonable agreement with the estimated value 0.27 eV [57] of the binding energy of an Na vacancy in the $Ca^{2+}V_{Na}^{-}$ dipole in the bulk of the crystal. Finally, at $E > 20$ kV m^{-1}, the growth of the velocity ceases, and v reaches saturation at a level of $\sim 2 \times 10^3 v_0$.

We emphasize that in the absence of a magnetic field ($B = 0$), the dislocations remain immobile at all amplitudes of the electric field. Therefore, in this case, undoubtedly, we are dealing with the effect of the electric field on the MPE rather than with the simple effect of the electric field on the mobility of dislocations. On the other hand, it follows from Eqn (11) that the only parameter on which the electric field can act is the number n_{act} of active Ca^+ centers at the dislocations. Judging from the data obtained, an electrostimulated thermofluctuational jump-like transfer of sodium vacancies from the $Ca^{2+}V_{Na}^{-}$ dipoles onto the edge of the extra half plane of the dislocation occurs with a simultaneous change in the charge of the calcium ion: $Ca^{2+} \rightarrow Ca^{+}$. As a result, with an increase in the field E, the number of active centers available for unzipping increases exponentially (see Fig. 4),

$$n_{act}(E) = n_{act}^0 \left[1 + \frac{E}{E_0} \exp\left(-\frac{U(E)}{k_B T}\right)\right], \tag{12}$$

and the mean unzipping length decreases accordingly.

Thus, the basic concept of the proposed kinematic model (11) that there is a large potential for a possible increase in the intensity of the MPE due to the growth of the number n_{act} of magnetically active Ca^+ centers finds experimental confirmation. We note incidentally that the electrical stimulation of the MPE was also recently discovered in LiF crystals [60].

5. Theoretical simulation of the hidden parameters of motion

When discussing experimental dependence (3) taking Eqn (11) into account, it must be assumed that the probability $w = n_{act}/n_{tot}$ depends on the impurity concentration C. At first glance, this assumption seems to be doubtful. The probability w is determined by the ratio of quantities each of which must grow with an increase in the concentration C of impurities. Why, under the conditions of our experiments, do they increase proportionally to each other? To answer this question, we pass to a discussion of the statistical properties of the system. These are not accessible to direct observations, and we therefore examine this problem theoretically and then, in Section 6, verify our conclusions with the aid of computer experiments on the simulation of magnetoplasticity.

5.1 Geometrical formulation of the problem

As was noted in Section 3, fresh dislocations in the experiments under consideration were introduced into the crystal by a light impact immediately before the measurements. The dislocations introduced in this way scatter away from the sources moving downward from the peaks of the potential landscape formed by the field corresponding to the pattern of long-range internal stresses σ_i until they reach places where the 'rolling-down' force of the landscape $F_i = b\sigma_i$ (per unit length of the dislocation) is compensated by the pinning force of impurity centers. When discussing the influence of the impurity concentration C on the results of these experiments, we should take into account that an increase in C leads to an increase in the number n_{tot} of stoppers on the dislocation and therefore in the pinning force as well. Thus, upon moving to the starting position, the dislocation stops earlier, at a location where the level of stress σ_i is higher. As we see below, under such conditions, for the dislocation carried out to the starting position, the proportionality condition

$$\sigma_i \propto n_{tot} \tag{13}$$

should be satisfied irrespective of the impurity concentration C.

We now discuss in more detail the problem of equilibrium and conditions necessary for a dislocation to detach from point defects. We assume that a dislocation of length L is retarded by n_{tot} identical stoppers, which are characterized by identical critical pinning forces f_c, and that the dislocation is detached from the defect when the force acting on the dislocation exceeds this pinning force. We assume for simplicity that the force $F_i = b\sigma_i$ acting per unit length of this dislocation is constant along its length. This simplifying assumption is plausible because the maximum contribution to the force F_i caused by internal stresses that act on this dislocation comes precisely from the dislocations that are parallel to it [61]. We assume that the related interactions are described in the approximation of linear tension, according to which all dislocation segments have the form of circular arcs of the same radius,

$$R = \frac{T}{F_i}, \tag{14}$$

where $T \sim Gb^2/(2\pi)$ is the linear tension force, proportional to the shear modulus G of the crystal. For further estimates, it is significant that the radius of curvature R in (14) is very large under the conditions of our experiments because of the high value of the ratio $G/\sigma_i \sim 10^5$. It can easily be shown that R is two orders of magnitude greater than the average length of the dislocation segment $\bar{x} \sim 1$ μm [see (26) in Section 5.3].

5.2 Condition of equilibrium and the criterion of the breakaway of a dislocation

We discuss the equilibrium of a dislocation in the field of long-range internal stresses simulated by an external force $F_i = b\sigma_i$ under the conditions of the retarding effect of point defects. As is shown in Fig. 3, the stopped dislocation 'hangs up' on the impurity stoppers, bending under the action of the force F_i. In the approximation accepted, the dislocation acts on the stopper n with a force $\mathbf{f}_n$ equal to the vector sum of two tensile forces caused by the adjacent segments, which make a bowing angle α_n between themselves. The magnitude of the force $\mathbf{f}_n$ is determined by the smaller diagonal of a rhombus with the side T (Fig. 5):

$$f_n = 2T\cos\frac{\alpha_n}{2} \approx T(\pi - \alpha_n) = 2T\theta_n, \tag{15}$$

[here, we took the smallness of the attack angle $\theta_n = (\pi - \alpha_n)/2$ into account].

Naturally, the following relations must be satisfied at equilibrium:

$$F_i \approx \frac{1}{L}\sum_{n=1}^{n_{tot}} f_n = \frac{2T}{L}\sum_{n=1}^{n_{tot}} \theta_n = \frac{2T\bar{\theta}}{L}\, n_{tot} = \frac{2T\bar{\theta}}{\bar{x}}, \tag{16}$$

where $\bar{x} = L/n_{tot}$ is the average length of the segment and $\bar{\theta}$ is the average value of the attack angle θ_n defined as

$$\bar{\theta} = \frac{1}{n_{tot}}\sum_{n=1}^{n_{tot}} \theta_n. \tag{17}$$

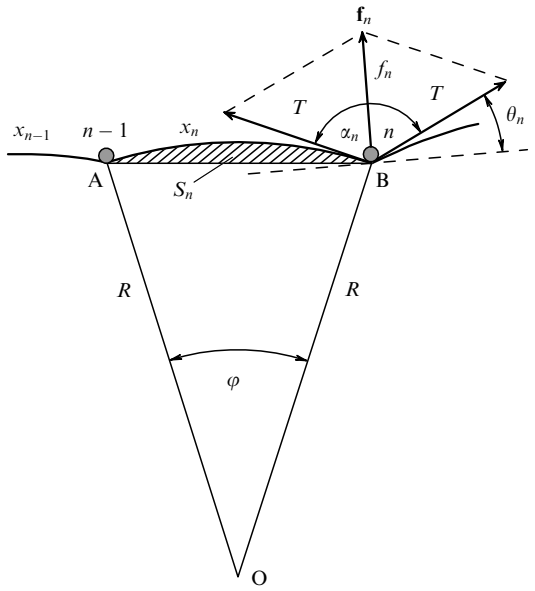

Figure 5. The force $\mathbf{f}_n$ acting on the nth stopper from the dislocation; α_n and θ_n are the respective angles of bowing and attack; S_n is the area swept by the dislocation before it is stopped.

In expression (16), we omit small corrections $\sim \bar{\theta}^3$ that take the nonorthogonality of the vectors $\mathbf{f}_n$ to the average direction of the dislocation into account. The accuracy of estimate (16) increases as the radius of curvature R (14) of the dislocation segments increases (see Fig. 5).

In our approximation, the short-range interaction of the impurity center with the dislocation is assumed to be a contact type, i.e., the pinning force that acts on the dislocation is assumed to have the form

$$J_n = \begin{cases} f_n\,, & f_n < f_c\,, \\ 0\,, & f_n > f_c\,. \end{cases} \tag{18}$$

Therefore, the condition of the equilibrium of the dislocation is the inequality

$$f_n < f_c\,,\ \text{i.e.,}\ \alpha_n > \alpha_c \approx \pi - \frac{f_c}{T}\ \text{ or }\ \theta_n < \theta_c = \frac{f_c}{2T}\,, \tag{19}$$

for all stoppers. We recall that in Eqns (18) and (19), f_c is the critical force acting on the stopper, the force at which the breakaway of the dislocation occurs. The proximity of the critical angle α_c to π is due to a very high linear tension T of the dislocation. As a result of this proximity, only insignificant deviations of the dislocation shape from linearity are possible.

Formulas (15)–(17) are valid at any under-threshold values of the external force F_i. At the same time, the criterion of the breakaway (loss of stability) of the dislocation is realized at a particular threshold value of the force $F_i = F_i^c$ at which the smallest bowing angle $\alpha_n^{\min}$ (and hence the highest attack angle $\theta_n^{\max} = \theta_m$) passes through its threshold value:

$$\alpha_n^{\min} = \alpha_c\,,\quad \theta_m = \theta_c\,,\ \text{i.e.,}\ f_n^{\max} = f_c = 2T\theta_c\,. \tag{20}$$

In this case, the quantities $\bar{x}$ and $\bar{\theta}$ in formula (16) for F_i correspond to the threshold configuration.

Certainly, the mean values $\bar{x}$ and $\bar{\theta}$ are the characteristics of a given configuration, and after the passage of the dislocation through a random distribution of point stoppers, the values of $\bar{x}$ and $\bar{\theta}$ should vary. Simultaneously, the total force of 'gliding friction' changes from a minimum value $F_{\min}$ to a maximum value $F_{\max}$. If the applied external force F_i is less than $F_{\min}$, the dislocation does not move; for $F_{\min} < F_i < F_{\max}$, the dislocation moves to some specific position; and, finally, at a supercritical level of the force $F_i > F_{\max}$, a total loss of stability occurs: the dislocation travels along the entire slip plane without stops. The motion of the dislocation under the conditions used in numerical experiments had just such a character (see Fig. 6 in Section 6.2).

However, a noticeable difference between the threshold forces $F_{\min}$ and $F_{\max}$ revealed in computer simulations is apparently caused by the relatively small total number of stoppers at the dislocation, $n_{\text{tot}} \sim 20-50$, which unavoidably should increase the dispersion of the measured parameters. In real experiments, this value was two orders of magnitude greater: $n_{\text{tot}} \sim 3 \times 10^3$. Furthermore, the measurements were carried out on well-annealed crystals, which ensured a high uniformity of the impurity distribution in the bulk. Under these conditions, the fluctuations of the mean values $\bar{x}$ and $\bar{\theta}$ must be small. Hence, in reality, the difference between $F_{\min}$ and $F_{\max}$ was insignificant. Therefore, all starting sites can be assumed to be precritical, when even a small decrease in the pinning force that acts on the dislocation in a magnetic field makes it move. This allows disregarding the dispersion of the mean values $\bar{x}$ and $\bar{\theta}$ in our estimations and expressing the critical force in accordance with formulas (16) and (20) as

$$F_i^c = b\sigma_i = \frac{\gamma f_c}{L}\, n_{\text{tot}} = \frac{\gamma f_c}{\bar{x}}\,, \tag{21}$$

where

$$\gamma = \frac{\bar{\theta}}{\theta_c}\,. \tag{22}$$

In computer experiments, such a critical state is apparently realized at $F_i^c = F_{\max}$ and is also described by formula (21). In (21) and (22), the critical parameters f_c and θ_c are characteristics of the type of stoppers and do not depend on their concentration C. The mean value of the attack angle $\bar{\theta}$ in the critical configuration can hardly be substantially dependent on C. As was confirmed by direct computer experiment, the parameter $\bar{\theta}$ and consequently γ are almost insensitive to changes in the concentration C, and we therefore assume that $\gamma = \text{const}$ in what follows.

Formula (21), in fact, refines relation (13). In Section 5.3, we refine it further and find the dependences of the key quantities σ_i and n_{tot} on the impurity concentration C.

5.3 Mean length of segments at the dislocation

The question about the mean length $\bar{x}$ of the segments at the dislocation is important and quite nontrivial. Intuitively, it is clear that for low internal stresses σ_i and an almost rectilinear dislocation, the length $\bar{x}$ should noticeably exceed the mean distance (9) between defects in the plane under consideration. It is also clear that the length $\bar{x}$ should depend both on the concentration of impurities C and on the stress σ_i. This is of fundamental importance for us because in this case expression (21) is converted from an estimate into an equation that contains σ_i in both the left- and right-hand sides. This is already a sufficient motivation for calculating the mean length $\bar{x}$.

For this, we consider the motion of a dislocation as the sweeping of an area in the slip plane on which defects are placed with a fixed density. The formation of a segment x_n occurs as follows. The dislocation, after meeting one stopper $(n-1)$ during its motion, bypasses it by bending around it until meeting another stopper (n), and then bends between them to the curvature radius $R = T/F_i$ (see Fig. 5). The swept area S_n (shown by hatching in Fig. 5) then contains one stopper (n) (the left-hand stopper $(n-1)$ is conventionally assigned to the segment x_{n-1}). If we are dealing with a segment with the mean length $\bar{x}$, then the product of the density of defects $2bC_V$ in the slip plane and the area S_n should give unity,

$$2bC_V S_n \approx 1\,. \tag{23}$$

The magnitude of S_n is found as the difference between the areas of the sector OAB and the triangle OAB in Fig. 5:

$$S_n = \frac{1}{2}\,R^2(\varphi - \sin\varphi) \approx \frac{1}{12}\,R^2\varphi^3 = \frac{\bar{x}^3}{12R}\,, \tag{24}$$

where we use the fact that $\varphi = \bar{x}/R$. It follows from Eqns (23) and (24) that

$$\bar{x} = \sqrt[3]{\frac{6R}{bC_V}} = \sqrt[3]{\frac{6T}{b^2C_V\sigma_i}} \approx \sqrt[3]{\frac{G}{C_V\sigma_i}}\,. \tag{25}$$

Using the values $G/\sigma_i \sim 10^5$ and $C_V \sim 10^{17}$ cm^{-3} for the NaCl crystal, we obtain the estimate

$$\bar{x} \sim 1\ \mu\text{m}\,. \tag{26}$$

We can now find the dependences $\sigma_i(C)$ and $n_{tot}(C)$. Substituting $\bar{x} = L/n_{tot}$ and the alternative expression $\bar{x} = \gamma f_c/(b\sigma_i)$, which follows from (21), in (25), we find

$$F_i^c = b\sigma_i \approx \sqrt{\frac{(\gamma f_c)^3}{bG}\,C_V}\,, \qquad n_{tot} \approx L\sqrt{\frac{\gamma f_c}{bG}\,C_V}\,. \tag{27}$$

Thus, the internal stress σ_i at the start and the total number of stoppers n_{tot} at the dislocation upon varying the impurity concentration C_V vary consistently proportionally to $\sqrt{C_V}$ but react differently to a change in the type of impurity: $\sigma_i \propto f_c^{3/2}$, but $n_{tot} \propto f_c^{1/2}$. In Section 6, these predictions are checked based on the results of computer simulations.

5.4 Distribution function of the pinning points depending on attack angles

We introduce the distribution function $H(\theta)$ of the pinning points at the dislocation depending on the attack angle θ:

$$\mathrm{d}n = n_{tot}H(\theta)\,\mathrm{d}\theta\,, \qquad \int_0^{\theta_c} H(\theta)\,\mathrm{d}\theta = 1\,. \tag{28}$$

In a simulation in Section 6, this function is reconstructed from the discrete histograms

$$\Delta n(\theta_l) = n_{tot}H(\theta_l)\Delta\theta\,. \tag{29}$$

With an increase in the concentration of stoppers C, the total number of pinning points n_{tot} at the dislocation increases, and the interval of the partition of the histogram $\Delta\theta$ remains unaltered, because the upper limit θ_c of attack angles in the histograms depends not on the concentration of the impurity, but on its type. It is obvious that the function $H(\theta)$ under condition (21) should also be independent of the concentration C. In Figs 3 and 5, the simultaneous change in $n_{tot} \propto F_i^c$ would then imply a simultaneous proportional change in all the lengths of the dislocation segments and in their curvature radii, which would influence only the scale of the figure rather than the distribution of angular characteristics in it. In other words, we have all grounds to believe that judging from the described experimental data, the distribution function $H(\theta)$ is not sensitive to changes in C. Certainly, this also relates to the mean values of the angles of bowing $\bar{\alpha}$ and attack angles $\bar{\theta}$, and to the parameter $\gamma = \bar{\theta}/\theta_c$, as is confirmed below based on the results of computer simulations (see the table in Section 6.3).

5.5 Independence of the relative number of magnetically active stoppers at the dislocation from the impurity concentration

As has already been noted, the magnetic transformation of a stopper weakens the pinning, i.e., reduces the critical threshold of the breakaway force f_c and consequently decreases the critical attack angle θ_c, which becomes $\theta_c^m < \theta_c$. If all the impurity centers were initially paramagnetic, then, in a time τ_{dp} after the application of the magnetic field, a breakaway of the dislocation would occur from all the stoppers for which the attack angle θ_n lies in the interval $\theta_c^m < \theta_n < \theta_c$. We recall that no equilibrium segment can fall into the supercritical range $\theta_n > \theta_c$. In terms of the distribution function $H(\theta)$, the number of such stoppers n_{act}^{pot} (potential unzipping centers after their magnetic transformation) is expressed as

$$n_{act}^{pot} = n_{tot}\int_{\theta_c^m}^{\theta_c} H(\theta)\,\mathrm{d}\theta\,. \tag{30}$$

However, as we could see in Section 3.3, there are serious experimental grounds to assume that for Ca impurities in the NaCl crystal, the above-found set of n_{act}^{pot} stoppers contains a mixture of Ca^{2+} and Ca^+ ions and that the first of them (magnetically nonactive) is absolutely predominant. Judging from all the above, the capture of an electron by a Ca^{2+} ion begins at the stoppers corresponding to the attack angles that significantly exceed the threshold angle θ_c^m. There is a more distinctive threshold value θ_c^+ of the attack angle for this process in the interval $\theta_c^m < \theta_c^+ < \theta_c$. The number of active centers Ca^+ at the dislocation is determined by a formula similar to (30):

$$n_{act}^{Ca^+} = n_{tot}\int_{\theta_c^+}^{\theta_c} H(\theta)\,\mathrm{d}\theta\,. \tag{31}$$

We emphasize that the threshold angles θ_c^+ and θ_c^m, just like the critical angle θ_c, are determined by the local properties of defects and are independent of their concentration.

The relation between the numbers in (30) and (31) can be estimated based on the experimental data [49, 50] given in Section 3.3. The saturation of the dislocation velocity observed at an enhanced strength of the electric field (see Fig.4c) apparently corresponds to the regime in which practically all centers at the dislocation are in the magnetically active state (Ca^+). The observed increase in the velocity v by a factor of approximately 2000 means, in view of Eqn (11), that the number n_{act}^{pot} in (30) is greater by the same factor than the spontaneous number of Ca^+ centers $n_{act}^{Ca^+}$

in (31), which are pinning centers in the absence of electroactivation: $n_{\rm act}^{\rm pot} \sim 2000 n_{\rm act}^{\rm Ca^+}$. Hence, in accordance with these experimental data, this number is greater than 20% of the total number of segments $n_{\rm tot} \sim 10^4$ located at the dislocations in the investigated NaCl crystals with the concentration of impurities ~ 10 ppm.

It is even more important for us that the probability

$$w = \frac{n_{\rm act}^{\rm Ca^+}}{n_{\rm tot}} = \int_{\theta_{\rm c}^+}^{\theta_{\rm c}} H(\theta)\,{\rm d}\theta \tag{32}$$

is independent of the impurity concentration C, which, with Eqn (11), is in complete agreement with the experimental dependence $l \propto 1/\sqrt{C}$ in Eqn (3). Thus, we have for the first time obtained a physical substantiation of this dependence.

6. Computer simulation of magnetoplasticity

6.1 Algorithms of numerical experiments

The motion of a dislocation in the slip plane of a crystal through a random network of point-like defects (pinning centers) was simulated as the displacement of a geometrical line in a two-dimensional space (slip plane) with chaotically located pinning points. In real experiments, well-annealed crystals with the density of point defects distributed sufficiently uniformly over the volume were used, and hence the arrangement of chaos in the distribution of points in the simulation region also excluded essential inhomogeneities in their density. In computer experiments, the number of stoppers N in the simulation region ranged from 500 to 2500. As was shown by estimates, this region approximately corresponds to the field of observation of a microscope with a diameter of several tens of microns.

The computer simulation was carried out as follows. The dislocation was moved from the starting position by small discrete steps toward an aggregate of point-like stoppers, remaining rectilinear until the first contact with one of them. At the instant of meeting, two auxiliary points were added outside the simulation region, which were located symmetrically with respect to this stopper relative to the left-hand and right-hand boundaries of the region, and the dislocation was bent to form two arcs on these three points. The midpoints of these arcs were moved along the left-hand and right-hand boundaries to their end positions corresponding to a specified curvature radius R. This radius was chosen, in accordance with (14), to be inversely proportional to a constant force F applied to the dislocation. In our dimensionless units, we assumed that $F = 1/R$. When one of the arcs reached the next stopper, it was also divided into two new arcs, and the motion continued according to the same rules. On the other side of each lateral boundary of the simulation region, an auxiliary point located symmetrically to the stopper at the dislocation nearest to this boundary was always added.

The breakaway from the defect n occurred when the angle of bowing α_n between the adjacent arcs (see Fig. 5) was smaller than the critical value $\alpha_{\rm c}$. Then the algorithm caused a step back, i.e., a return to the configuration that preceded the approach of the dislocation to this point. The further calculations were continued without taking the existence of this point into account. The computation process stopped when the dislocation passed through all pinning points or when all the arcs reached their minimum radius $R = 1/F$ in the absence of the angles of bowing α_n smaller than the critical angle $\alpha_{\rm c}$. This configuration was regarded as the starting position in our simulation.

By varying the parameters N, F, and $\alpha_{\rm c}$, their combinations were found that carry the dislocation to the starting configuration necessary for further numerical experiments, simulating the motion of the dislocation in a magnetic field. Furthermore, the statistical properties of the starting configuration have been studied, including the distribution function of the attack angles θ_n and different relations between the parameters that were predicted above.

The algorithm of 'switching on' the magnetic field consisted in the following. At the dislocation in the equilibrium starting position, all pinning centers simultaneously changed their depinning threshold: their critical angle $\alpha_{\rm c}$ increased by a specific value $\Delta\alpha_{\rm c}$. In this case, the critical attack angle $\theta_{\rm c} = (180^\circ - \alpha_{\rm c})/2$ in the magnetic field decreased to

$$\theta_{\rm c}^{\rm m} = \theta_{\rm c} - \frac{1}{2}\,\Delta\alpha_{\rm c}\,. \tag{33}$$

We selected the angle $\theta_{\rm c}^{\rm m}$ to be proportional to $\theta_{\rm c}$, varying it in the limits

$$\theta_{\rm c}^{\rm m} = (0.2{-}0.3)\theta_{\rm c}\,. \tag{34}$$

The increase in the angle $\Delta\alpha_{\rm c}$ then turned out to be proportional to $\theta_{\rm c}$:

$$\Delta\alpha_{\rm c} = (0.7{-}0.8)2\theta_{\rm c}\,. \tag{35}$$

After the magnetic field was switched on, part of the stoppers at the dislocation with the angles of bowing in the range $\theta_{\rm c}^{\rm m} < \theta_n < \theta_{\rm c}$ became unstable, and the breakaway of dislocations occurred precisely at these stoppers. In terms of Section 5.5, such stoppers are called active. In the framework of our algorithm, the other stoppers, still before a dislocation reached them, were returned to the original value of the critical angle $\alpha_{\rm c}$. This allowed accounting for the processes in which some of the defects can be overcome without the delay necessary for their magnetic transformation. The dislocation then moved in the usual regime until it reached the next stoppage in a new equilibrium configuration. Here, the magnetic field was switched on again, and so on. Each stoppage was fixed as a delay equal to the duration of the occurrence of the process of magnetic transformation of the defect $\tau_{\rm dp}$. All the other processes were considered instantaneous.

6.2 Simulation of taking a dislocation to the starting position

Figure 6 shows a number of dependences of dislocation displacements on the applied force F for different values of the critical angle $\alpha_{\rm c}$ and for three values of the total number of stoppers: $N = 500$, 1500, and 2500. As can be seen from the figure, the motion occurs as a process of loss of stability. At values of the force F smaller than a particular threshold value $F_{\rm min}$, the dislocation barely moves, remaining in the initial position. At $F > F_{\rm min}$, the dislocation mean path increases smoothly with increasing F to a certain critical value $F = F_{\rm max} \equiv F_{\rm c}$, which depends on the number N of stoppers and on the critical angle $\alpha_{\rm c}$. The smoothness of the behavior of

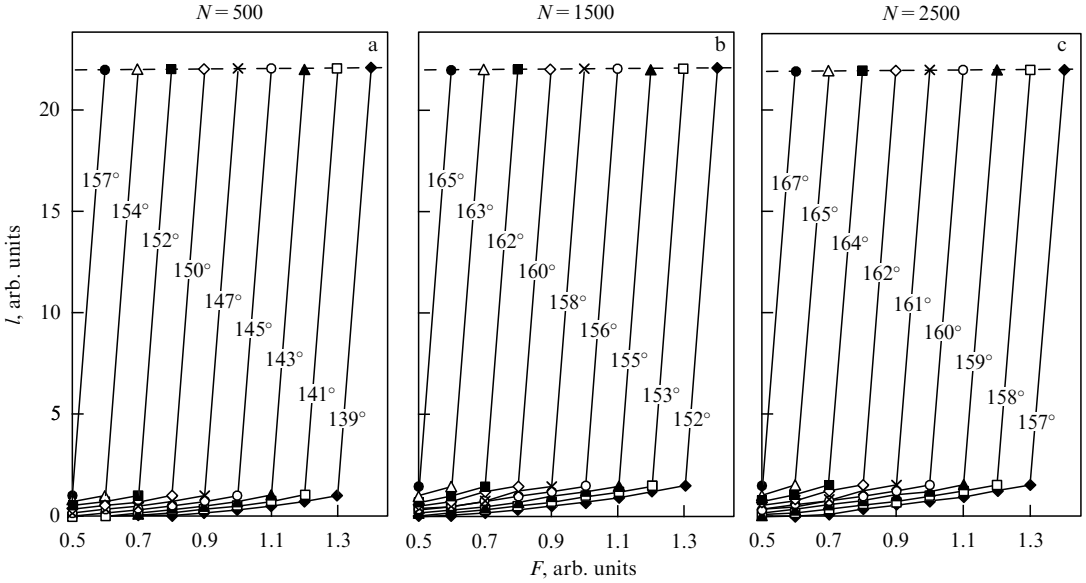

Figure 6. Equilibrium positions l of a dislocation upon increasing the force F to the value $F = F_c$ corresponding to the loss of stability, for different critical bowing angles α_c and the number of stoppers N: (a) 500, (b) 1500, and (c) 2500.

the dislocation terminates at this configuration. With a further increase in F, however small, the dislocation loses stability, 'rushing' through the remaining obstacles over the entire region of simulation.

In terms of Section 5.2, the dislocation reaches a critical configuration at $F = F_c$, which is an analog of taking the dislocation to the starting position in experiment. The critical force F_c apparently corresponds to the above quantity $F_i^c = b\sigma_i$ in the starting position. The existence of a threshold force F_c, which is fixed at constant values of the critical attack angle $\theta_c \propto f_c$ in (20) and the total number of stoppers $N \propto C_V$, already confirms the basic concept developed in Section 5.3. However, formula (27) gives more detailed predictions of the concrete types of dependence of this force on θ_c and N:

$$F_c = k\theta_c^{3/2}, \qquad k \propto \sqrt{N}. \tag{36}$$

The dependences $F_c(\theta_c, N)$ obtained by processing the results of the numerical experiments presented in Fig. 6 and of similar data obtained at $N = 1000$ and 2000 are given in the straightening coordinates in Fig. 7. It can be seen that analytic expectations (36) are corroborated quite satisfactorily. This agreement of the simplified theory with the results of simple computer experiments allows us to hope that our conclusions are reliable and can be used to analyze the results of physical experiments and the data on magnetoplasticity among them.

The obtained critical configurations of dislocations before the loss of stability at the corresponding values of F_c and the same set of the numbers N allow finding the $n_{tot}(\theta_c, N)$ dependences and comparing them with analytic prediction (27), according to which

$$n_{tot} = k\sqrt{\theta_c}, \qquad k \propto \sqrt{N}. \tag{37}$$

Such a comparison is given in Fig. 8 in the straightening coordinates, and is quite satisfactory. In particular, the linear dependence of n_{tot} on $\sqrt{N}$ shown in Fig. 8b, together with the data in Fig. 7b, confirm the predicted directly

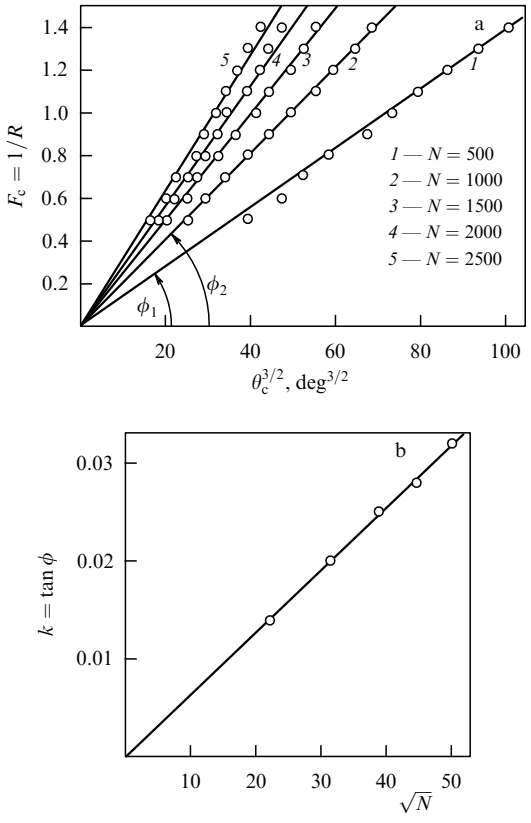

Figure 7. Dependences of the threshold force F_c on (a) the critical attack angle and (b) the number of stoppers N in the straightening coordinates, in accordance with formula (36).

proportional variation (13) of the pinning stress σ_i and of the number n_{tot} with a change in the impurity concentration and therefore confirm the version of the theory advanced in Section 5, which explains the observed dependence of the dislocation mean path $l \propto 1/\sqrt{C}$ (3) obtained in real experiments.

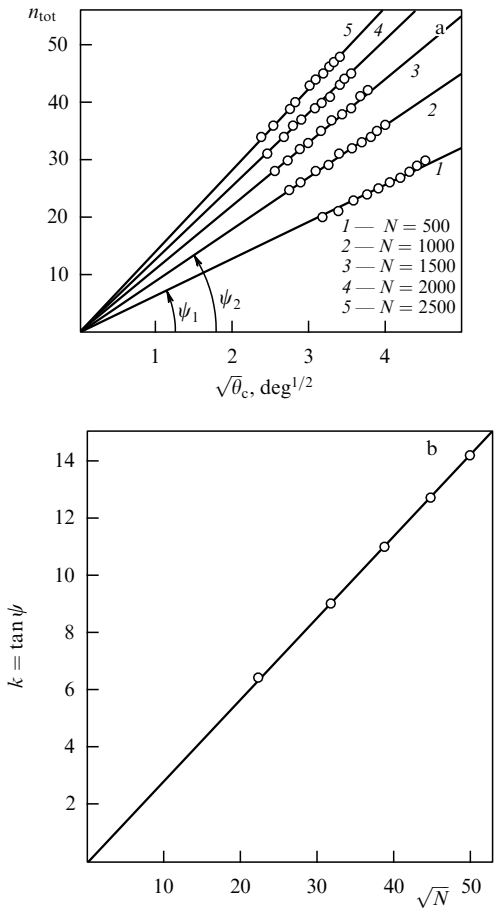

Figure 8. Dependence of the average number n_{tot} of stoppers at a dislocation on (a) the critical attack angle θ_c and (b) the number of stoppers N in the straightening coordinates, in accordance with formula (37).

6.3 Distribution of stoppers at a dislocation depending on the attack angle

The obtained critical configurations of a dislocation that lie at the basis of the constructions shown in Fig. 8 allow extracting additional information on the distributions of dislocation pinning points depending on the bending angle α_n or the attack angles θ_n. In Fig. 9, the discrete points show normalized histograms of distributions over attack angles $H(\theta_n)$ described by formula (29). As an example, one such histogram is shown that corresponds to $N = 1500$. The total range $0 < \theta < \theta_c$ was divided into eight equal intervals of width $\Delta\theta = \theta_c/8$. The symbols placed in Fig. 9 at the centers of these intervals correspond to the magnitudes of $H(\theta_n)$ in each of them for different N. For a fixed critical angle $\theta_c = 11.5°$, i.e., for one type of stoppers, the density of stoppers was varied as in natural experiments (see Fig. 1). Five values of the total number of stoppers were used: $N = 500$, 1000, 1500, 2000, and 2500. The parameters n_{tot} necessary for the calculation of the normalized values of $H(\theta_n)$ for each of these five N are given in the table.

From the histogram shown in Fig. 9, we can easily obtain the mean attack angle

$$\bar{\theta} = \sum_{n=1}^{8} \theta_n H(\theta_n) \Delta\theta \qquad (38)$$

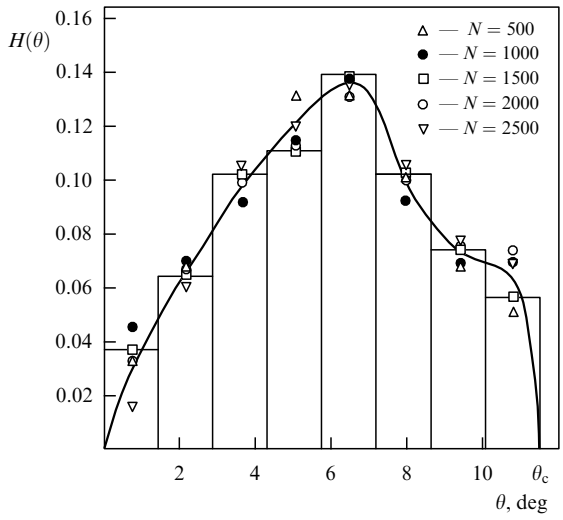

Figure 9. Discrete values $H(\theta_n)$ of the distribution function of attack angles found at $N = 500$, 1000, 1500, 2000, and 2500 from normalized histograms similar to that given in the figure for $N = 1500$; the solid curve shows the approximation of the function $H(\theta)$ defined by (28).

Table 1. Characteristics of the critical dislocation starting configurations simulated at $\alpha_c = 157°$ for different values of the total number of stoppers N.

N	500	1000	1500	2000	2500
$F_i = 1/R$	0.50	0.80	0.95	1.10	1.30
n_{tot}	21	31	37	43	48
$\bar{\theta}$, deg	10.030	10.100	10.030	10.035	10.035
$\gamma = \bar{\theta}/\theta_c$	0.873	0.878	0.873	0.873	0.873

and the corresponding ratio $\gamma = \bar{\theta}/\theta_c$. As can be seen from Table 1, both parameters are virtually independent of the number of obstacles N, which, however, was actually expected according to the theoretical consideration expounded in Section 5.4.

Even more importantly we see the proximity between all normalized histograms corresponding to different N; within their statistical variability, their envelope (shown in Fig. 9 by the solid curve) yields a universal distribution function of attack angles $H(\theta)$, as was predicted. We note that each histogram was obtained from a single experiment, and therefore the statistical variability of the points in Fig. 9 is natural. Undoubtedly, averaging the histograms over multiple experiments would practically eliminate this variability.

6.4 Simulation of the dislocation motion in a magnetic field

In simulating the motion of dislocations in a magnetic field, we ignore such complexities as the need for preliminary transformation $Ca^{2+} \rightarrow Ca^{+}$ of the impurity pinning centers into the magnetically sensitive state. It is assumed for simplicity that the impurity pinning centers are already in the paramagnetic state. In this sense, our algorithm describes the experiments presented in Section 4.3, with a simultaneously acting electric field $E > 20$ kV m^{-1}, when this state already exists.

The importance of the simulation does not, naturally, reduce to only the reproduction of experimental data. Our purpose is to trace the hidden features of the phenomenon

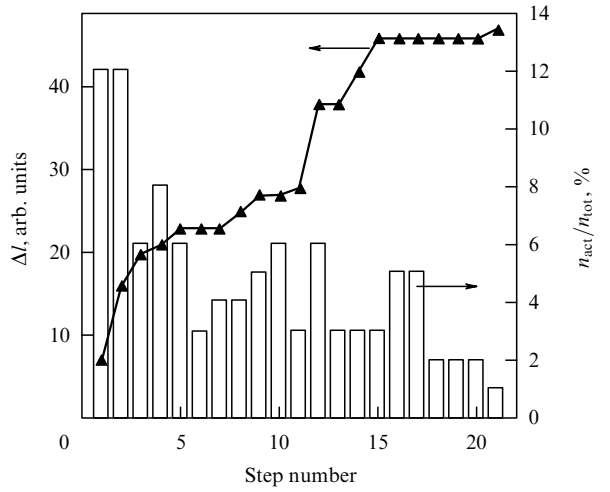

Figure 10. Simulated sequential positions of a dislocation in its stops that require the switching-on of the magnetic field to continue the motion (left-hand vertical axis), and the relative number of active centers that are overcome due to the effect of the magnetic field (right-hand vertical axis): $N = 2000$; the critical bending angle $\theta_c = 7.5°$, which decreases in the magnetic field to $\theta_c^m = 2°$.

studied, those not visible in real experiments, and to answer the question of whether the key concepts of the kinematic scheme proposed above on the basis of indirect data are valid. Here, we check whether the unzipping (sequential lateral 'unbuttoning') is a typical feature of the process of magneto-induced displacements of dislocations.

Figure 10 shows the results of simulation of the dislocation motion through a network of randomly distributed point-like stoppers ($N = 2000$) with the critical attack angle $\theta_c = 7.5°$, which decreases in the magnetic field to $\theta_c^m = 2°$. Along the horizontal axis, the sequential stops of the dislocation motion are indicated, each of which requires the switching-on of the magnetic field to continue motion. In fact, this axis corresponds to the discrete time in our simulation, because the time is required in our simulation scheme only for the magnetically induced breakaway. The left-hand vertical axis shows the positions of a dislocation at a given particular instant (positions of the 'points of etching'). Along the right-hand vertical axis, the relative number of active pinning points (centers of unzipping), which free the dislocations when the magnetic field is switched on, are given as the percentage of the total number n_{tot} of pinning centers. With an organization of the simulation data, it is possible not only to trace the average position of a dislocation (position of the 'etching pit') but also to have information about the number of centers of magneto-induced unzipping at each particular time instant.

As can be seen from Fig. 10, the number of magnetic unzipping centers is rather small ($\sim 10\%$ on average), which reminds us of our estimate of the number of such centers under the effect of the accompanying electric field $E > 20$ kV m^{-1} (see Section 5.5): $n_{act}^{pot}/n_{tot} \sim 20\%$.

The presence of unzipping is also confirmed by the curve of free paths in Fig. 10. We see horizontal regions on this curve, below which there are columns corresponding to the normal magnetic activity of stoppers at the dislocations. This completely corresponds to the image of the constant positions of the etching pits on the surface to which the unzipping wave has not yet arrived.

7. Conclusions

In this article, we concentrated on the study of the kinematical aspect of magnetoplasticity, disregarding the deep physics of complex spin-related processes underlying the phenomenon. The experimental study of these complex processes is possible only to the extent to which it is possible to trace the cause-and-effect relations between the different-scale processes. It is necessary to build a bridge between the observed displacements of dislocations (10–100 μm) and spin processes in a huge number of impurity centers of atomic dimensions. This task was set out in this investigation.

In solving this problem, we relied on the results of diverse real observations (see Sections 3 and 4) in combination with the results of new theoretical models (see Section 5) and a specially implemented computer simulation that allows extracting important information about hidden parameters that cannot be found experimentally (see Section 6). We emphasize that combining the data of 'real' and numerical experiments turned out to be very fruitful. We can also assert that the proposed kinematic scheme sufficiently successfully explains practically all results observed in model crystals of NaCl. Moreover, this model successfully passed a nontrivial test such as the interpretation of the increase in the velocity of motion of dislocations by three orders of magnitude under the effect of an additional action of a relatively weak electric field, about 10 kV m^{-1} (see Section 4.3).

As was noted in Section 2, the magnetic transformation of the structure of point defects can affect not only mechanical but also some other physical properties of crystals. Modification of the dielectric properties of ferroelectrics in a magnetic field was already noticed long ago [62–66]. In recent years, more systematic studies of this range of phenomena began [67–69]. There are grounds to believe that these types of effects are based on changes in the pinning of domain walls by structure defects modified by the magnetic field. Apparently, we are dealing here with phenomena that have a common physical foundation. However, the explanation of the kinematics of processes of this type is a matter for the future.

As regards the ultrafast coherent relaxation of the dislocation structure in NaCl crystals revealed to us in Earth's magnetic field under the conditions of resonance pulsed pumping, through which almost all dislocations could travel macroscopic distances of the order of 100 μm in a time of approximately 0.5 μs [37], we recall the correlations, noted long ago, between earthquakes and disturbances of the geomagnetic field. In recent years, such correlations have been confirmed by a serious statistical analysis carried out by well-known specialists in seismology. Apparently, there is a trigger-type action of such disturbances, which starts a 'catastrophic' drop in the internal stresses. It is quite possible that here we studied concrete physical mechanisms of a similar trigger effect (see, e.g., [70]).

Certainly, the magnetoresonance transformations of defects as a general phenomenon can imply some other hazards. For example, they can lead to a degradation of critical elements of constructions and devices, when the effects due to Earth's weak magnetic field are combined with background fields in the radio-frequency range. Similar processes can also occur in protein structures. In magneto-biology, different aspects of the influence of weak magnetic fields on physiological processes have already been investigated [71, 72].

Acknowledgments
The authors are grateful to A Yu Belov and S A Minyukov for the useful discussions of different aspects of our work at various stages. The work was supported in part by a grant from the presidium of the Russian Academy of Sciences (program of basic research no. 1).

References

1. Alshits V I, Darinskaya E V, Perekalina T M, Urusovskaya A A *Sov. Phys. Solid State* **29** 265 (1987); *Fiz. Tverd. Tela* **29** 467 (1987)
2. Alshits V I, Darinskaya E V, Petrzhik E A *Izv. Vyssh. Uchebn. Zaved. Chern. Metallurg.* (10) 85 (1990)
3. Alshits V I, Darinskaya E V, Petrzhik E A *Sov. Phys. Solid State* **33** 1694 (1991); *Fiz. Tverd. Tela* **33** 3001 (1991)
4. Molotskii M I *Sov. Phys. Solid State* **33** 1760 (1991); *Fiz. Tverd. Tela* **33** 3112 (1991)
5. Salikhov K M, Molin Yu N, Buchachenko A L, Sagdeev R Z *Spin Polarization and Magnetic Effects in Radical Reactions* (Amsterdam: Elsevier, 1984); Translated from Russian: Buchachenko A L, Sagdeev R Z, Salikhov K M *Magnitnye i Spinovye Effekty v Khimicheskikh Reaktsiyakh* (Magnetic and Spin Effects in Chemical Reactions) (Novosibirsk: Nauka, 1978)
6. Zel'dovich Ya B, Buchachenko A L, Frankevich E L *Sov. Phys. Usp.* **31** 385 (1988); *Usp. Fiz. Nauk* **155** 3 (1988)
7. Alshits V I, Darinskaya E V, Koldaeva M V, Petrzhik E A *Crystallogr. Rep.* **48** 768 (2003); *Kristallogr.* **48** 826 (2003)
8. Urusovskaya A A, Alshits V I, Smirnov A E, Bekkauer N N *Crystallogr. Rep.* **48** 796 (2003); *Kristallogr.* **48** 855 (2003)
9. Golovin Yu I *Phys. Solid State* **46** 789 (2004); *Fiz. Tverd. Tela* **46** 769 (2004)
10. Morgunov R B *Phys. Usp.* **47** 125 (2004); *Usp. Fiz. Nauk* **174** 131 (2004)
11. Alshits V I, Darinskaya E V, Koldaeva M V, Petrzhik E A, in *Dislocations in Solids* (Ed. J P Hirth) Vol. 14 (Amsterdam: Elsevier, 2008) p. 333
12. Alshits V I et al. *JETP Lett.* **63** 668 (1996); *Pis'ma Zh. Eksp. Teor. Fiz.* **63** 628 (1996)
13. Golovin Yu I et al. *JETP Lett.* **68** 426 (1998); *Pis'ma Zh. Eksp. Teor. Fiz.* **68** 400 (1998)
14. Golovin Yu I et al. *JETP* **90** 939 (2000); *Zh. Eksp. Teor. Fiz.* **117** 1080 (2000)
15. Alshits V I, Darinskaya E V, Petrzhik E A *Phys. Solid State* **35** 162 (1993); *Fiz. Tverd. Tela* **35** 320 (1993)
16. Alshits V I, Darinskaya E V, Gektina I V, Lavrent'ev F F *Sov. Phys. Crystallogr.* **35** 597 (1990); *Kristallogr.* **35** 1014 (1990)
17. Alshits V I, Darinskaya E V, Petrzhik E A *Sov. Phys. Solid State* **34** 81 (1992); *Fiz. Tverd. Tela* **34** 155 (1992)
18. Darinskaya E V, Petrzhik E A, Erofeeva S A, Kisel' V P *JETP Lett.* **70** 309 (1999); *Pis'ma Zh. Eksp. Teor. Fiz.* **70** 298 (1999)
19. Golovin Yu I, Morgunov R B *JETP Lett.* **61** 596 (1995); *Pis'ma Zh. Eksp. Teor. Fiz.* **61** 583 (1995)
20. Urusovskaya A A, Alshits V I, Smirnov A E, Bekkauer N N *JETP Lett.* **65** 497 (1997); *Pis'ma Zh. Eksp. Teor. Fiz.* **65** 470 (1997)
21. Smirnov B I, Peschanskaya N N, Nikolaev V I *Phys. Solid State* **43** 2250 (2001); *Fiz. Tverd. Tela* **43** 2154 (2001)
22. Tyapunina N A, Krasnikov V L, Belozerova É P *Phys. Solid State* **41** 942 (1999); *Fiz. Tverd. Tela* **41** 1035 (1999)
23. Smirnov A E, Urusovskaya A A *Sov. Phys. Solid State* **29** 485 (1987); *Fiz. Tverd. Tela* **29** 852 (1987)
24. Golovin Yu I, Morgunov R B *JETP Lett.* **58** 191 (1993); *Pis'ma Zh. Eksp. Teor. Fiz.* **58** 189 (1993)
25. Golovin Yu I et al. *Phys. Status Solidi A* **160** R3 (1997)
26. Golovin Yu I et al. *JETP Lett.* **69** 127 (1999); *Pis'ma Zh. Eksp. Teor. Fiz.* **69** 114 (1999)
27. Darinskaya E V et al. *Phys. Status Solidi C* **2** 1873 (2005)
28. Petrzhik E A, Darinskaya E V, Dem'yanets L N *Phys. Solid State* **50** 638 (2008); *Fiz. Tverd. Tela* **50** 614 (2008)
29. Osip'yan Yu A et al. *JETP Lett.* **69** 123 (1999); *Pis'ma Zh. Eksp. Teor. Fiz.* **69** 110 (1999)
30. Koldaeva M V, Turskaya T N, Darinskaya E V *Crystallogr. Rep.* **50** 278 (2005); *Kristallogr.* **50** 312 (2005)
31. Osip'yan Yu A et al. *JETP Lett.* **79** 126 (2004); *Pis'ma Zh. Eksp. Teor. Fiz.* **79** 158 (2004)
32. Badylevich M V et al. *Phys. Status Solidi C* **2** 1869 (2005)
33. Alshits V I et al. *JETP Lett.* **91** 91 (2010); *Pis'ma Zh. Eksp. Teor. Fiz.* **91** 97 (2010)
34. Alshits V I et al. *Phys. Solid State* **53** 2117 (2011); *Fiz. Tverd. Tela* **53** 2010 (2011)
35. Alshits V I, Darinskaya E V, Koldaeva M V, Petrzhik E A *Phys. Solid State* **55** 358 (2013); *Fiz. Tverd. Tela* **55** 318 (2013)
36. Alshits V I, Darinskaya E V, Koldaeva M V, Petrzhik E A *Phys. Solid State* **54** 324 (2012); *Fiz. Tverd. Tela* **54** 305 (2012)
37. Alshits V I et al. *Phys. Solid State* **55** 2289 (2013); *Fiz. Tverd. Tela* **55** 2176 (2013)
38. Alshits V I et al. *JETP Lett.* **98** 28 (2013); *Pis'ma Zh. Eksp. Teor. Fiz.* **98** 33 (2013)
39. Alshits V I et al. *JETP Lett.* **99** 82 (2014); *Pis'ma Zh. Eksp. Teor. Fiz.* **99** 87 (2014)
40. Koldaeva M V et al. *Bull. Russ. Acad. Sci. Phys.* **78** 1086 (2014); *Izv. Ross. Akad. Nauk Ser. Fiz.* **78** 1341 (2014)
41. Alshits V I et al. *Bull. Russ. Acad. Sci. Phys.* **78** 1041 (2014); *Izv. Ross. Akad. Nauk Ser. Fiz.* **78** 1294 (2014)
42. Morgunov R B *Phys. Solid State* **53** 786 (2011); *Fiz. Tverd. Tela* **53** 733 (2011)
43. Alshits V I, Darinskaya E V *JETP Lett.* **70** 761 (1999); *Pis'ma Zh. Eksp. Teor. Fiz.* **70** 749 (1999)
44. Molotskii M, Fleurov V *Phys. Rev. B* **63** 132102 (2001)
45. Molotskii M, Fleurov V *Phys. Rev. B* **63** 184421 (2001)
46. Buchachenko A L *JETP* **102** 795 (2006); *Zh. Eksp. Teor. Fiz.* **129** 909 (2006)
47. Buchachenko A L *JETP* **105** 593 (2007); *Zh. Eksp. Teor. Fiz.* **132** 673 (2007)
48. Buchachenko A L *JETP* **105** 722 (2007); *Zh. Eksp. Teor. Fiz.* **132** 827 (2007)
49. Alshits V I, Darinskaya E V, Koldaeva M V, Petrzhik E A *JETP Lett.* **88** 428 (2008); *Pis'ma Zh. Eksp. Teor. Fiz.* **88** 500 (2008)
50. Alshits V I, Darinskaya E V, Koldaeva M V, Petrzhik E A *J. Appl. Phys.* **105** 063520 (2009)
51. Alshits V I, Darinskaya E V, Koldaeva M V, Petrzhik E A *JETP* **122** 118 (2016); *Zh. Eksp. Teor. Fiz.* **149** 136 (2016)
52. Belyavsky V I, Levin M N *Phys. Rev. B* **70** 104101 (2004)
53. Morgunov R B, Buchachenko A L *JETP* **109** 434 (2009); *Zh. Eksp. Teor. Fiz.* **136** 505 (2009)
54. Morgunov R B, Buchachenko A L *Phys. Rev. B* **82** 014115 (2010)
55. Kotowski R, Alshits V, Tronczyk P *Przeglad Elektrotechniczny* **82** (12) 80 (2006)
56. Golovin Yu I et al. *Phys. Solid State* **39** 554 (1997); *Fiz. Tverd. Tela* **39** 634 (1997)
57. Lidiard A B "Ionic conductivity", in *Electrical Conductivity II* (Handbuch der Physik, Vol. 20, Ed. S von Flügge) (Berlin: Springer-Verlag, 1957) p. 246; Translated into Russian: *Ionnaya Provodimost' Kristallov* (Moscow: IL, 1962)
58. Zakrevskii V A, Pakhotin V A, Shul'diner A V *Phys. Solid State* **44** 2083 (2002); *Fiz. Tverd. Tela* **44** 1990 (2002)
59. Galustashvili M V et al. *Phys. Solid State* **58** 557 (2016); *Fiz. Tverd. Tela* **58** 543 (2016)
60. Galustashvili M V et al. *Phys. Solid State* **55** 1676 (2013); *Fiz. Tverd. Tela* **55** 1565 (2013)
61. Alshits V I, Darinskaya E V, Koldaeva M V *Phys. Solid State* **43** 1703 (2001); *Fiz. Tverd. Tela* **43** 1635 (2001)
62. Flerova S A, Bochkov O E *JETP Lett.* **33** 34 (1981); *Pis'ma Zh. Eksp. Teor. Fiz.* **33** 37 (1981)
63. Levin M N et al. *Phys. Solid State* **45** 542 (2003); *Fiz. Tverd. Tela* **45** 513 (2003)
64. Levin M N, Postnikov V V, Palagin M Yu *Phys. Solid State* **45** 1763 (2003); *Fiz. Tverd. Tela* **45** 1680 (2003)
65. Levin M N, Postnikov V V, Palagin M Yu *Tech. Phys. Lett.* **29** 444 (2003); *Pis'ma Zh. Tekh. Fiz.* **29** (12) 62 (2003)
66. Lashley J C et al. *Appl. Phys. Lett.* **90** 052910 (2007)
67. Petrzhik E A, Ivanova E S, Alshits V I *Bull. Russ. Acad. Sci. Phys.* **78** 1052 (2014); *Izv. Ross. Akad. Nauk Ser. Fiz.* **78** 1305 (2014)
68. Yakushkin E D *JETP Lett.* **99** 415 (2014); *Pis'ma Zh. Eksp. Teor. Fiz.* **99** 483 (2014)
69. Ivanova E S, Rumyantsev I D, Petrzhik E A *Phys. Solid State* **58** 127 (2016); *Fiz. Tverd. Tela* **58** 125 (2016)
70. Buchachenko A L *Phys. Usp.* **57** 92 (2014); *Usp. Fiz. Nauk* **184** 101 (2014)
71. Binhi V N, Savin A V *Phys. Usp.* **46** 259 (2003); *Usp. Fiz. Nauk* **173** 265 (2003)
72. Buchachenko A L *Russ. Chem. Rev.* **83** 1 (2014); *Usp. Khim.* **83** 1 (2014)